

Article

Synergetic Effect of Ni₂P/SiO₂ and γ-Al₂O₃ Physical Mixture in Hydrodeoxygenation of Methyl Palmitate

Ivan V. Shamanaev ^{1,*} , Irina V. Deliy ¹ , Evgeny Yu. Gerasimov ^{1,2}, Vera P. Pakharukova ¹, Evgeny G. Kodenev ¹, Pavel V. Aleksandrov ¹ and Galina A. Bukhtiyarova ¹

¹ Borekov Institute of Catalysis, Lavrentieva Ave. 5, 630090 Novosibirsk, Russia; delij@catalysis.ru (I.V.D.); gerasimov@catalysis.ru (E.Y.G.); verapakharukova@yandex.ru (V.P.P.); kodenev_e@mail.ru (E.G.K.); aleksandrov@catalysis.ru (P.V.A.); gab@catalysis.ru (G.A.B.)

² Department of Physics, Novosibirsk National Research University, Pirogova St. 2, 630090 Novosibirsk, Russia

* Correspondence: i.v.shamanaev@catalysis.ru; Tel.: +7-383-326-9410

Received: 9 October 2017; Accepted: 31 October 2017; Published: 6 November 2017

Abstract: The Ni₂P/SiO₂ catalyst, which was prepared by in situ temperature-programmed reduction and in the mixture with the inert (SiC, SiO₂) or acidic (γ-Al₂O₃) material was studied in methyl palmitate hydrodeoxygenation (HDO). Methyl palmitate HDO was carried out at temperatures of 270–330 °C, H₂/feed volume ratio of 600 Nm³/m³, and H₂ pressure of 3.0 MPa. Ni₂P/SiO₂ catalyst, diluted with γ-Al₂O₃ showed a higher activity than Ni₂P/SiO₂ catalyst diluted with SiC or SiO₂. The conversion of methyl palmitate increased significantly in the presence of γ-Al₂O₃ most probably due to the acceleration of the acid-catalyzed reaction of ester hydrolysis. The synergism of Ni₂P/SiO₂ and γ-Al₂O₃ in methyl palmitate HDO can be explained by the cooperation of the metal sites of Ni₂P/SiO₂ and the acid sites of γ-Al₂O₃ in consecutive metal-catalyzed and acid-catalyzed reactions of HDO. The obtained results let us conclude that the balancing of metal and acid sites plays an important role in the development of the efficient catalyst for the HDO of fatty acid esters over supported phosphide catalysts.

Keywords: nickel phosphide; biofuel; hydrodeoxygenation; aliphatic esters; synergetic effect; alumina

1. Introduction

In the last decade, the development of new catalytic technologies that produce liquid transportation fuels from renewables has seen a growing interest due to the depletion of available fossil fuel resources and environmental issues [1–8]. Hydroprocessing of triglyceride-based feedstock, including non-edible vegetable oils, tall oils, animal fats, and waste frying oils is an efficient way to produce diesel and aviation fuel components [3,9–13]. Elimination of oxygen from the triglyceride molecules proceeds through the different competing routes [11,12,14–16]: hydrodeoxygenation (HDO) or decarboxylation/decarbonylation (DeCO_x). Water molecules and alkanes with the same number of carbon atoms are produced in the HDO pathway, while the DeCO_x reactions give CO_x molecules and alkanes with the shorter carbon chains. The hydroprocessing of triglyceride-based feedstock gives the mixture of C₁₅–C₁₈ paraffins, called green or renewable diesel. This product is fully compatible with fossil-derived diesel fuel; it has a high cetane number and good stability. The use of green diesel improves the engine fuel economy and reduces the harmful emission when it is used in the mixture with the fossil-derived fuels [11,17,18].

Until recently, the catalysts containing sulphide Co(Ni)Mo phase [15–17,19–24] or noble metals [4,19,25–29] were intensively investigated in HDO of the real feedstock and model compounds. Despite the high activity of noble metal catalysts, the high cost and shortage of noble metal restricted their practical application. For hydrotreating catalysts, a sulphiding agent should be continuously fed

to the reaction mixture to prevent deactivation [30]. Besides, water and carbon oxides can negatively influence the catalytic properties of supported noble metal and metal sulphide catalysts [31–33].

To avoid the disadvantages of supported noble metals and sulphide catalysts, several new types of systems containing supported base metals, preferentially Ni [13,34–39], or base metal carbides [40–42], nitrides [43], and phosphides [44–54] were investigated in HDO. In particular, the nickel phosphide catalysts exhibit the high activity and stability in the HDO of model compounds [44,46,48,50,55–66] and vegetable oils [51,67], as well as in co-hydrotreatment of renewable oils with petroleum-derived distillates [68].

Long-chain fatty acids and their esters are usually selected as model compounds because of their structural similarity and common features of catalysts behaviour in the transformation of esters, and specific and natural triglycerides [69,70]. Under HDO conditions, corresponding carboxylic acids, aldehydes, alcohols, and alkenes are usually observed among the intermediate compounds of aliphatic esters conversion. HDO of aliphatic esters into hydrocarbons proceeds through a complicated reaction network, including hydrogenation-dehydrogenation, hydrogenolysis of C–O and C–C bonds, hydrolysis, dehydration, and esterification reaction [11,16,19,44,71]. Both metallic and acid-base properties play an important role in the transformation of the aliphatic ester into acid, which could proceed through hydrogenolysis of C–O bond of ester group over metallic sites or through acid-catalyzed hydrolysis. It was proposed that the conversion of ester to carboxylic acids could proceed with participation of Brønsted acid sites of silica-supported nickel phosphide [44,47,56,57,62]. Besides, the Lewis acid sites of the alumina support were presumed to enhance the rate of hydrolysis of aliphatic esters over sulphide catalysts [20,21]. It was observed that the reaction rate of ethyl stearate HDO over Ru/TiO₂ catalyst was enhanced by the addition of γ -Al₂O₃ [26], but this phenomenon was not clarified.

The above consideration let us propose that the use of the alumina support instead of silica could improve the catalytic activity of the supported phosphide catalysts in aliphatic ester conversion, but the preparation of Ni₂P/ γ -Al₂O₃ catalysts with the highly dispersed uniform phosphide nanoparticles is a complicated task. The strong interaction between phosphate groups and alumina surface hinders the reduction and impedes the formation of alumina-supported nickel phosphide [72–74]. Zhang et al. [65] have observed that AlPO₄ forms after TPR of Ni₂P/ γ -Al₂O₃ precursors, and Ni/ γ -Al₂O₃ shows a higher activity than Ni₂P/ γ -Al₂O₃.

To overcome this drawback and to verify the hypothesis about the enhancement of esters conversion rate in the presence of alumina, the catalytic properties of supported Ni₂P/SiO₂ catalyst mixed with the inert material (SiC or SiO₂) or acidic support (γ -Al₂O₃) were compared in HDO of methyl palmitate. It was found that catalytic activity of Ni₂P/SiO₂ catalyst in methyl palmitate HDO was enhanced strongly in the presence of γ -Al₂O₃. The analysis of the product distribution in liquid and gas phase depending on temperature and contact time allowed us to suggest a possible route of methyl palmitate transformation caused by Lewis acid sites of alumina surface.

2. Results and Discussion

2.1. Catalyst Characterization

The characteristics of Ni₂P/SiO₂ sample reduced in a quartz tubular reactor ex situ and catalyst after catalytic experiment are presented in Table 1.

According to the inductively coupled plasma atomic emission spectroscopy (ICP-AES) data, all of the samples after reduction contained comparable amounts of Ni about 2.5 wt % with Ni/P molar ratio approaching 2, whereas the precursor obtained after calcination at 500 °C for 4 h contained the Ni/P ratio approaching 0.6 which is close to the initial ratio in the impregnation solution (0.5). The Ni/P molar ratios obtained from Energy Dispersive X-ray Analysis of phosphide nanoparticles by the TEM are about 1.5–1.6, the discrepancy with bulk ICP-AES (chemical analysis) may be due to the locality of the transmission electron microscopy (TEM) method. The difference in Ni/P molar

phosphorus in the form of volatile phosphorous-containing compounds (P_4 , PH_3 , P_2H_6 , etc.) during the temperature-programmed reduction of NiP_xO_y/SiO_2 precursor [75–77]. PH_3 or P_2H_6 species produced in course of temperature-programmed reduction (TPR) could react with nickel-containing oxide precursors [78] or metallic Ni, resulting in nickel phosphide formation [79–81].

Table 1. Physicochemical properties of the calcined NiP_xO_y/SiO_2 precursor and Ni_2P/SiO_2 catalysts.

Sample	Ni (wt %)	Ni/P Molar Ratio (from EDX ²)	D_{TEM} (nm)
NiP_xO_y/SiO_2	2.6 ± 0.3	-	-
reduced ex situ Ni_2P/SiO_2	2.5 ± 0.2	1.5 ± 0.1	3.6 ± 0.8
Spent ¹ Ni_2P/SiO_2	2.5 ± 0.2	1.6 ± 0.1	3.3 ± 0.7

¹ After reaction in mixture with SiC; ² EDX: Energy Dispersive X-ray Analysis.

The specific surface area and pore volume of Ni_2P/SiO_2 catalyst are decreased in comparison with the SiO_2 support ($254 \text{ m}^2/\text{g}$ vs. $300 \text{ m}^2/\text{g}$ of SiO_2 , and $0.66 \text{ cm}^3/\text{g}$ vs. $0.80 \text{ cm}^3/\text{g}$ of SiO_2), while the average pore diameter is virtually the same (10.5 nm in contrast to 10.6 nm of SiO_2).

The X-ray Diffraction (XRD) patterns of the Ni_2P/SiO_2 catalysts after ex situ reduction and after catalytic experiment are shown in Figure 1. The diffraction pattern of the Ni_2P/SiO_2 catalysts after ex situ reduction shows the diffraction lines ($2\theta=40.71^\circ$, 44.61° , 47.36° , 54.18° , 54.99°) corresponding to nickel phosphide, Ni_2P (JCPDS powder diffraction file, card #03-0953). In addition, there is a broad halo at $2\theta \sim 15\text{--}30^\circ$ attributed to amorphous silica. The XRD pattern of the Ni_2P/SiO_2 catalyst used in the catalytic reaction additionally contained the peaks characteristic for the diluent, SiC, whose fine grains cannot be separated completely. Nickel phosphide phase was not changed in the course of the reaction (Figure 1, Table 1).

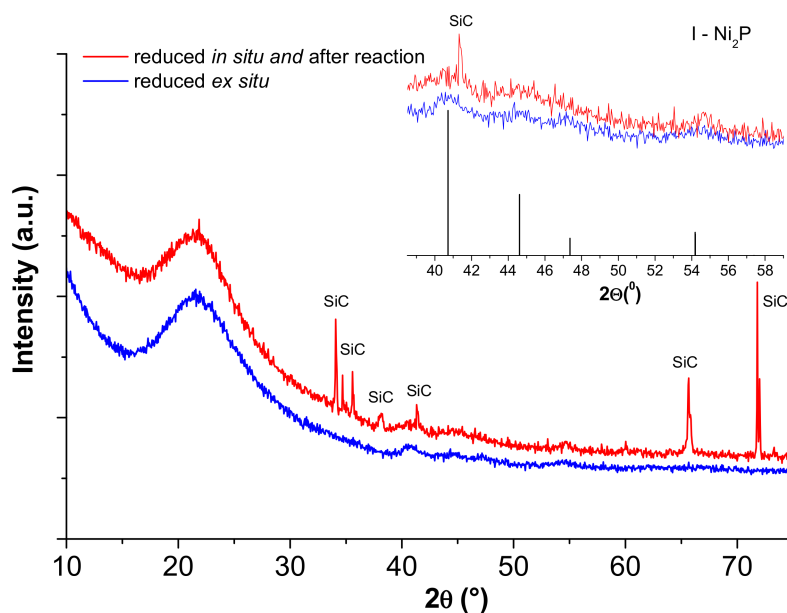


Figure 1. XRD patterns of Ni_2P/SiO_2 catalysts obtained by ex situ reduction and by in situ reduction and exposed to the catalytic reaction.

Figure 2 shows the TEM micrographs of ex situ reduced Ni_2P/SiO_2 sample (Figure 2A), and spent Ni_2P/SiO_2 catalyst after testing in the mixture with SiC (Figure 2B). Nickel phosphide particles that are uniformly distributed on the surface of silica are observed in the TEM images of both samples, with the similar particle sizes distribution and the mean particles sizes of Ni_2P (D_{TEM}) equal to $3.6 \pm 0.8 \text{ nm}$ and $3.3 \pm 0.7 \text{ nm}$, correspondingly. The TEM image of Ni_2P/SiO_2 catalyst (see Figure S1 in Supplementary

Materials) reveals crystal lattice fringes with the d-spacing value of 2.05 Å corresponding to the (201) reflection of the Ni₂P crystalline phase (JCPDS #03-0953). According to the TEM data, the parameters of the nickel phosphide phase were not changed significantly after testing in the methyl palmitate HDO, as well as the Ni/P ratio determined in the phosphide particles by means of Energy Dispersive X-ray Analysis (EDX) (Table 1).

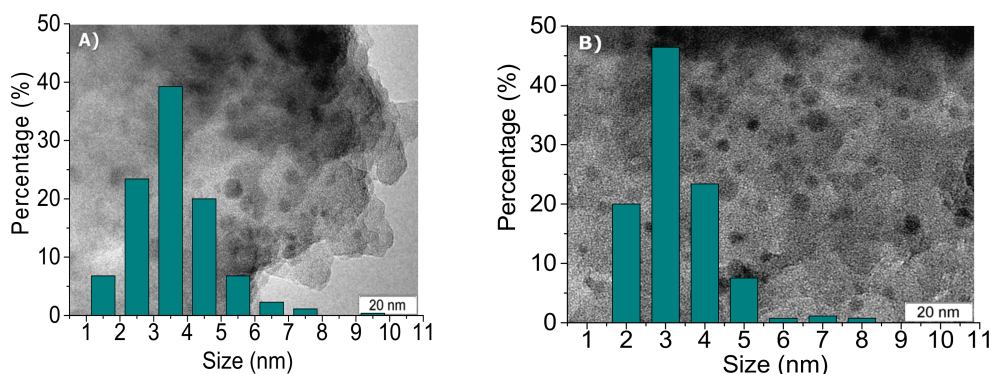


Figure 2. Transmission electron microscopy (TEM) micrographs and particles size distribution of Ni₂P/SiO₂ catalysts obtained by ex situ reduction (A) and by in situ reduction and exposed to the catalytic reaction (B).

To explore the acidic properties of applied materials (Ni₂P/SiO₂ catalyst, as well as SiO₂ and γ -Al₂O₃), the NH₃-TPD technique was employed. Prior to NH₃-TPD experiments, the Ni₂P/SiO₂ catalyst was reduced in situ at 600 °C for 1 h in H₂ flow to avoid the contact with air. This technique helps to get away possible oxidation of nickel phosphide during passivation and/or transfer to Autosorb-1 apparatus. Figure 3 shows the temperature-programmed desorption of ammonia (NH₃-TPD) profiles of Ni₂P/SiO₂ catalyst, SiO₂, and γ -Al₂O₃ samples. Ni₂P/SiO₂ catalyst and SiO₂ support show only one peak corresponding to weak acidic sites with T_{\max} at 231 °C [61,82–84]. The total quantities of acid sites estimated by integration of NH₃ desorption peaks are summarized in Table 2. The total acidity of Ni₂P/SiO₂ catalyst is equal to 110 μ mol/g. That was by 31% more than the acidity of the silica support. It is known that in case of silica-supported nickel phosphide catalysts, PO_x groups are responsible for the weak Brønsted acidity of Ni_xP_y/SiO₂ catalysts [47,82,83].

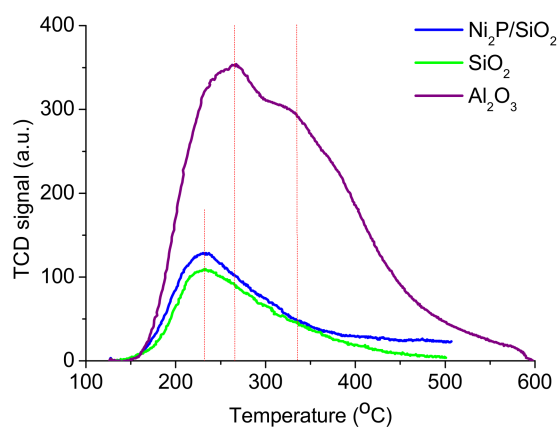


Figure 3. Temperature-programmed desorption of ammonia (NH₃-TPD) profiles of Ni₂P/SiO₂ catalyst, silica (SiO₂), and acidic support (γ -Al₂O₃) samples.

Table 2. The characteristics of Ni₂P/SiO₂ catalyst, SiO₂, and γ -Al₂O₃ samples.

Sample	$T_{\text{reduction}}, ^\circ\text{C}$	NH ₃ -TPD	
		$T_{\text{max}}, ^\circ\text{C}$	Quantity, $\mu\text{mol/g}$
SiO ₂	-	231	84
Ni ₂ P/SiO ₂	600	231	110
γ -Al ₂ O ₃	-	237	106
		335	315

On NH₃-TPD curve of applied γ -Al₂O₃, two desorption peaks of ammonia centered at 237 and 335 °C were observed. The first desorption peak around 237 °C belongs to sites with the weakest acidity responsible for physisorbed and chemisorbed ammonia. The second desorption peak at the temperature of 337 °C was assigned to the moderate strength acid sites [85]. According to literature [86,87], γ -Al₂O₃ shows typical Lewis acidity. It is clearly seen from our results that alumina displays higher amount of acid sites in comparison with the Ni₂P/SiO₂ catalyst.

2.2. Hydrodeoxygenation of Methyl Palmitate over Ni₂P/SiO₂ Catalyst

Figure 4 shows the conversions of methyl palmitate and oxygen-containing compounds in the temperature range of 250–330 °C over Ni₂P/SiO₂-SiC, Ni₂P/SiO₂-SiO₂, and Ni₂P/SiO₂- γ -Al₂O₃ physical mixtures. Ni₂P/SiO₂ catalyst and diluent were taken in a volume proportion of 1:8.2. In these experiments, the conversions of methyl palmitate and oxygen-containing compounds are increased with the temperature growth overall studied systems; wherein, the Ni₂P/SiO₂- γ -Al₂O₃ mixture displays the highest activity in the whole temperature range. The temperature dependencies of methyl palmitate conversion over Ni₂P/SiO₂-SiC and Ni₂P/SiO₂-SiO₂ do not significantly differ. Common features in the behaviour of these systems are the minor differences between the curves of methyl palmitate conversion and conversion of oxygen-containing compounds. A visible difference (1–2%) is observed only at temperatures of 250 and 270 °C, indicating the formation of minor amounts of oxygen-containing intermediates in the course of methyl palmitate HDO over Ni₂P/SiO₂ catalyst mixed with the inert materials, such as SiO₂ or SiC. In these cases, the negligible amounts of oxygen-containing compounds are observed among the reaction products (Figure 5). Such behaviour led us to the conclusion that over Ni₂P/SiO₂-SiC and Ni₂P/SiO₂-SiO₂ systems, the rate of methyl palmitate conversion is much lower than the rates of further reaction steps of oxygenated intermediates conversion. As a consequence, the methyl palmitate initial transformation determines the rate of methyl palmitate HDO over Ni₂P/SiO₂-SiC and Ni₂P/SiO₂-SiO₂ systems.

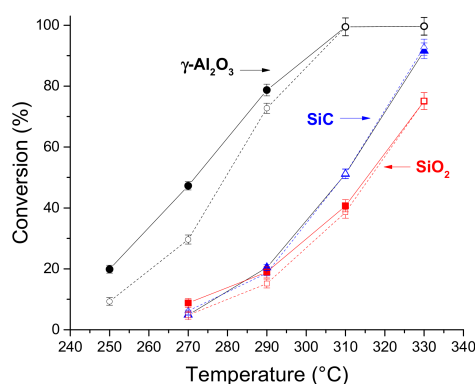


Figure 4. Effect of temperature on the conversions of methyl palmitate (solid symbols, solid lines) and oxygen-containing compounds (empty symbols, dash lines) over Ni₂P/SiO₂-SiC (triangles), Ni₂P/SiO₂-SiO₂ (squares) and Ni₂P/SiO₂- γ -Al₂O₃ (circles) systems. Reaction conditions: P_{H_2} —3.0 MPa, H_2/feed —600 Nm³/m³, weight hourly space velocity (WHSV)—5 h⁻¹.

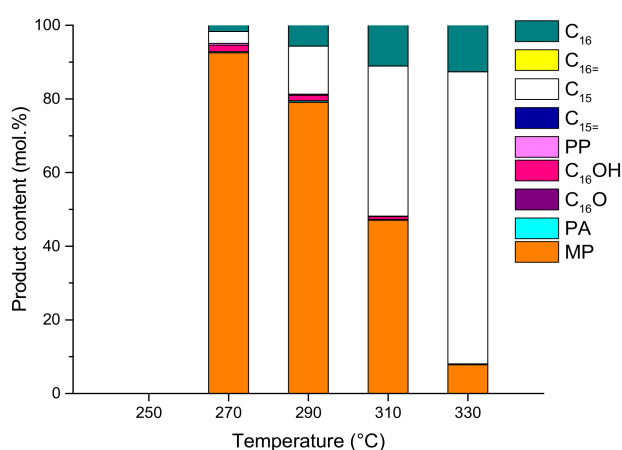


Figure 5. Effect of temperature on the composition of the liquid feed obtained in the HDO of methyl palmitate over $\text{Ni}_2\text{P}/\text{SiO}_2\text{-SiC}$ system. Reaction conditions: P_{H_2} —3.0 MPa, H_2/feed — $600 \text{ Nm}^3/\text{m}^3$, WHSV — 5 h^{-1} . MP—methyl palmitate ($\text{C}_{15}\text{H}_{31}\text{COOCH}_3$), PA—palmitic acid ($\text{C}_{15}\text{H}_{31}\text{COOH}$), C_{16}O —hexadecanal ($\text{C}_{15}\text{H}_{31}\text{CHO}$), C_{16}OH —hexadecanols ($\text{C}_{16}\text{H}_{33}\text{OH}$), PP—palmityl palmitate ($\text{C}_{15}\text{H}_{31}\text{COOC}_{16}\text{H}_{33}$), $\text{C}_{15}=\text{}$ —pentadecene ($\text{C}_{15}\text{H}_{30}$), $\text{C}_{15}\text{-}n$ —pentadecane ($\text{C}_{15}\text{H}_{32}$), $\text{C}_{16}=\text{}$ —hexadecane ($\text{C}_{16}\text{H}_{32}$), $\text{C}_{16}\text{-}n$ —hexadecane ($\text{C}_{16}\text{H}_{34}$).

Completely different behaviour in HDO of methyl palmitate is demonstrated by $\text{Ni}_2\text{P}/\text{SiO}_2\text{-}\gamma\text{-Al}_2\text{O}_3$ system. First of all, the activity of $\text{Ni}_2\text{P}/\text{SiO}_2$ catalyst is increased sharply when acidic $\gamma\text{-Al}_2\text{O}_3$ is used instead of the inert diluents. At 290 °C, the methyl palmitate conversion reaches 78.7% in comparison with 20.4% and 18.9% obtained over $\text{Ni}_2\text{P}/\text{SiO}_2\text{-SiC}$ and $\text{Ni}_2\text{P}/\text{SiO}_2\text{-SiO}_2$ systems (Figure 4). Then, a noticeable gap is observed between the conversion of methyl palmitate and the conversion of oxygen-containing compounds over $\text{Ni}_2\text{P}/\text{SiO}_2\text{-}\gamma\text{-Al}_2\text{O}_3$, along with the appreciable amounts of oxygenated intermediates detected among the reaction products at the reaction temperature of 250, 270, and 290 °C (Figures 4–6). The observed results reveal that the conversion of methyl palmitate over $\text{Ni}_2\text{P}/\text{SiO}_2\text{-}\gamma\text{-Al}_2\text{O}_3$ system precedes with a higher rate than the conversion of intermediate oxygenates. The possible routes of methyl palmitate transformation should be analyzed to clarify the possible reasons of methyl palmitate conversion acceleration in the presence of $\gamma\text{-Al}_2\text{O}_3$.

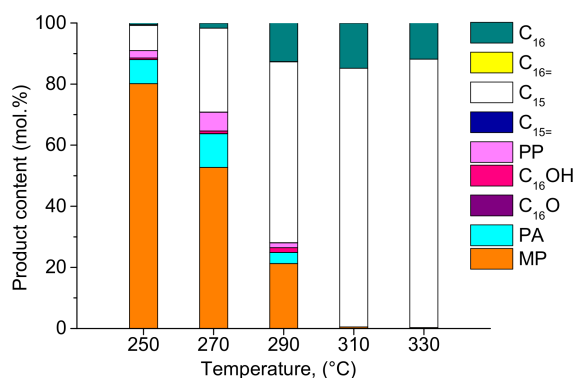
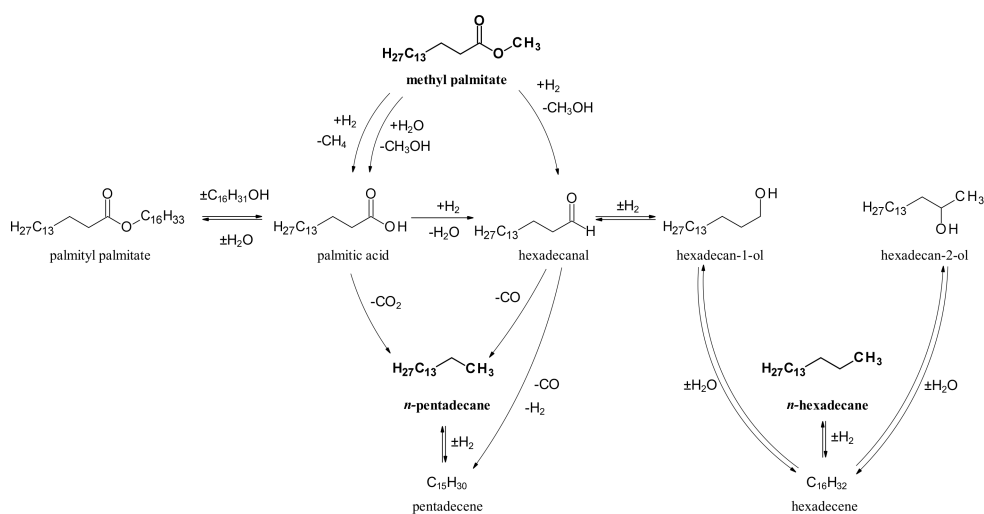


Figure 6. Effect of temperature on the composition of the liquid feed obtained in the HDO of methyl palmitate over $\text{Ni}_2\text{P}/\text{SiO}_2\text{-}\gamma\text{-Al}_2\text{O}_3$ system. Reaction conditions: P_{H_2} —3.0 MPa, H_2/feed — $600 \text{ Nm}^3/\text{m}^3$, WHSV — 5 h^{-1} . MP—methyl palmitate ($\text{C}_{15}\text{H}_{31}\text{COOCH}_3$), PA—palmitic acid ($\text{C}_{15}\text{H}_{31}\text{COOH}$), C_{16}O —hexadecanal ($\text{C}_{15}\text{H}_{31}\text{CHO}$), C_{16}OH —hexadecanols ($\text{C}_{16}\text{H}_{33}\text{OH}$), PP—palmityl palmitate ($\text{C}_{15}\text{H}_{31}\text{COOC}_{16}\text{H}_{33}$), $\text{C}_{15}=\text{}$ —pentadecene ($\text{C}_{15}\text{H}_{30}$), $\text{C}_{15}\text{-}n$ —pentadecane ($\text{C}_{15}\text{H}_{32}$), $\text{C}_{16}=\text{}$ —hexadecane ($\text{C}_{16}\text{H}_{32}$), $\text{C}_{16}\text{-}n$ —hexadecane ($\text{C}_{16}\text{H}_{34}$).

Several routes of conversion of methyl esters of fatty acids over silica-supported nickel phosphide catalysts were discussed in the literature [14,44–48,50,53,56,57,60,63,65,74,88,89]. The proposed schemes were based on the distributions of the reaction products in the liquid and gas phases vs. methyl palmitate conversion (or weight hourly space velocity (WHSV)). The main products of methyl palmitate HDO over Ni₂P/SiO₂ catalysts were hexadecane and pentadecane; palmitic acid, hexadecanal, hexadecanols, palmityl palmitate, unsaturated C₁₅₌, and C₁₆₌ hydrocarbons were identified as the intermediate products. Methane, CO, and methanol were observed in the gas phase.

The generally accepted reactions of methyl palmitate include hydrogenolysis of the C–O bond in the methoxy group giving CH₄ and the corresponding acid, as well as hydrogenolysis of the ester C–O bond, leading to aldehyde and methanol (Scheme 1). Along with the hydrogenolysis reactions, hydrolysis of ester giving the acid and methanol as a result of ester and water interaction is also considered [56,57,62,64,65]. The acid P–OH groups of Ni₂P particles supported on silica have been proposed to provide the hydrolysis reaction [44,46]. Further conversion of palmitic acid could theoretically proceed through the decarboxylation reaction giving pentadecane or through the hydrogenation to hexadecanal. The proceeding of the first reaction over Ni₂P/SiO₂ catalysts is unlikely because no CO₂ has been observed in the outlet gas [44,46,56,57]. Hexadecanal can be transformed into the C₁₅ or C₁₆ hydrocarbons. Decarbonylation and dehydroformylation reactions give pentadecane and pentadecene, while hydrogenation of hexadecanal produces hexadecane-1-ol, which is transformed to hexadecane through the subsequent dehydration and hydrogenation. Palmityl palmitate has also been identified in a small amount due to the acid-catalyzed reversible esterification reaction.



Scheme 1. Proposed reaction network of methyl palmitate hydrodeoxygenation (HDO) over Ni₂P/SiO₂.

The yields of palmitic acid and palmityl palmitate increase noticeably when γ -Al₂O₃ is used instead of inert SiC in the mixture with the Ni₂P/SiO₂ catalyst (Figure 6). The increase in palmitic acid yield indicates the increasing rates of reaction producing palmitic acid. Hydrogenolysis reactions are unlikely over Lewis acid sites of alumina without hydrogen-supplying metal sites in close proximity. Only small amounts of oxygenated products without any alkane were obtained over alumina in the same conditions. The concept of hydrogen spillover from metal sites of Ni₂P to the ester or other reagents adsorbed on the alumina surface is also doubtful; R. Prins in his review [90] has called into question the availability of hydrogen spillover from a metal surface to the surface of a non-reducible supports, such as γ -Al₂O₃, SiO₂, MgO, and zeolites. The most reliable explanation is based on the idea that the conversion rate of methyl palmitate increases due to Lewis acidity of alumina, which is known to provide the acid-catalyzed reaction, such as hydrolysis, dehydration, and esterification [60,74].

The hydrolysis of methyl palmitate proceeds on the Lewis acid sites of alumina, increasing the rate of methyl palmitate conversion. Besides, the proceeding of other acid-catalyzed reactions is observed in the presence of $\gamma\text{-Al}_2\text{O}_3$, providing the additional support of the proposed hypothesis. The product distribution in the gas phase obtained at a nearly complete conversion of methyl palmitate (99.7% conversion is reached over $\text{Ni}_2\text{P}/\text{SiO}_2\text{-}\gamma\text{-Al}_2\text{O}_3$ system and 91.6%—over $\text{Ni}_2\text{P}/\text{SiO}_2\text{-SiC}$ at 330 °C) is shown in Figure 7. Dimethyl ether appears among the gas phase products of methyl palmitate HDO when $\gamma\text{-Al}_2\text{O}_3$ was used instead of SiC as a diluent, pointing out to the proceeding of the acid-catalyzed reaction. On the other hand, the quantity of CO is nearly the same, confirming the negligible impact of alumina on the decarbonylation reaction. CO_2 is also found but in amounts by two orders of magnitude less than CO, so the contribution of the decarboxylation reaction can be neglected. Methane is produced in a smaller amount in the presence of $\gamma\text{-Al}_2\text{O}_3$, and this observation can be considered as an indirect indication of methane origin through the hydrogenation of methanol rather than via hydrogenolysis of the C–O bond in the methoxy group. Some amount of methanol is consumed by the formation of dimethyl ether over Lewis acid sites of alumina instead of hydrogenation to methane.

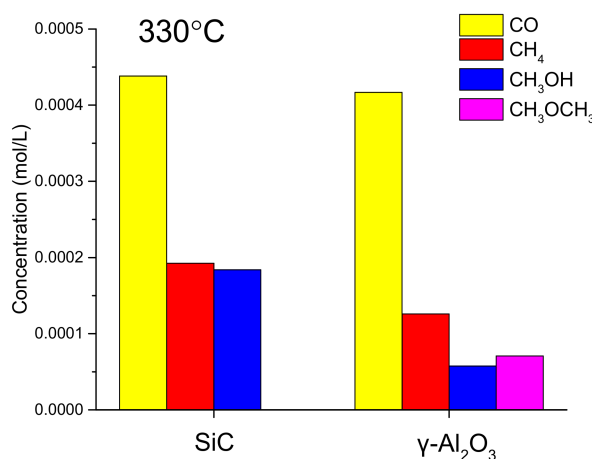


Figure 7. The composition of the gas phase products of methyl palmitate HDO obtained over $\text{Ni}_2\text{P}/\text{SiO}_2\text{-}\gamma\text{-Al}_2\text{O}_3$ system (at 99.7% conversion of MP) and $\text{Ni}_2\text{P}/\text{SiO}_2\text{-SiC}$ (at 91.6% conversion of MP). Reaction conditions: P_{H_2} —3.0 MPa, H_2/feed — $600 \text{ Nm}^3/\text{m}^3$, WHSV — 5 h^{-1} .

The yield of palmitic acid decreases and the yield of palmityl palmitate increases with the proceeding of the reaction due to the reversible esterification of palmitic acid with hexadecanol (Figure 8). The esterification and dehydrogenation reactions compete for hexadecanol; as a consequence, it is observed only in a small amount in the studied range of reaction conditions (Figure 6, Figure 7, Figure 8). Reversible palmityl palmitate hydrolysis starts only after the complete consumption of palmitic acid, the produced palmitic acid, and hexadecanol are converted, as described earlier. Hexadecan-2-ol is also observed among the reaction products that can be produced through the dehydration of hexadecan-1-ol and subsequent hydration of hexadecene to hexadecan-2-ol. Concentrations of hexadecan-1-ol and hexadecan-2-ol were summed to give hexadecanols yield.

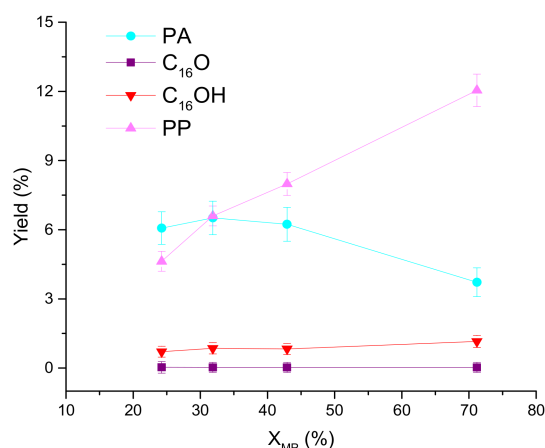


Figure 8. Yields of oxygenated intermediates vs. X_{MP} over $Ni_2P/SiO_2-\gamma-Al_2O_3$ system Reaction conditions: P_{H_2} —3.0 MPa, $H_2/$ feed—600 Nm^3/m^3 , T —270 °C, WHSV—5 h^{-1} . PA—palmitic acid ($C_{15}H_{31}COOH$), $C_{16}O$ —hexadecanal ($C_{15}H_{31}CHO$), $C_{16}OH$ —hexadecanols ($C_{16}H_{33}OH$), PP—palmityl palmitate ($C_{15}H_{31}COOC_{16}H_{33}$).

Summarizing the described results, we have proposed that synergism of Ni_2P/SiO_2 and $\gamma-Al_2O_3$ physical mixture in methyl palmitate HDO is provided by the additional conversion of the initial ester through the hydrolysis over Lewis acid sites of alumina. The further balancing of the metal sites of Ni_2P/SiO_2 and acid sites of $\gamma-Al_2O_3$ in one reactor can increase the activity of the catalytic systems. An apparent lag was observed between methyl palmitate conversion and overall oxygen-containing compounds conversion over the $Ni_2P/SiO_2-\gamma-Al_2O_3$ system. This indicates a lower rate of the metal-catalyzed reactions. To reduce this imbalance, a higher amount of Ni_2P/SiO_2 catalyst was used in the catalytic experiments: the Ni_2P/SiO_2 catalyst and $\gamma-Al_2O_3$ were taken in the proportion of 1:3.6 instead of 1:8.2.

Figure 9 shows the conversions of methyl palmitate and oxygen-containing compounds in the temperature range of 250–330 °C over $Ni_2P/SiO_2-\gamma-Al_2O_3$ physical mixtures with the catalyst and $\gamma-Al_2O_3$ volume ratio of 1:8.2 and 1:3.6. The increase of catalyst portion in the reactor results in the evident growth of methyl palmitate conversion, which is provided by the cooperation of metal and acid sites in the methyl palmitate HDO through the complicated set of acid-catalyzed and metal-catalyzed reactions.

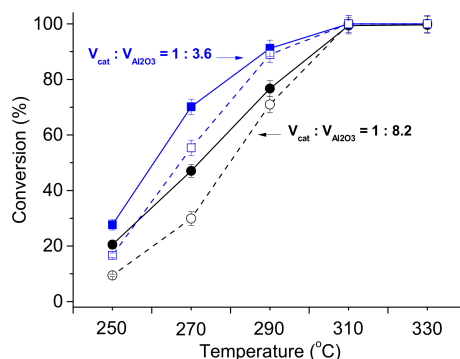


Figure 9. Effect of temperature on the conversions of methyl palmitate (solid symbols, solid lines) and oxygen-containing compounds (empty symbols, dash lines) over $Ni_2P/SiO_2-\gamma-Al_2O_3$ systems with different $V_{cat}:V_{Al_2O_3}$ ratio. Reaction conditions: P_{H_2} —3.0 MPa, $H_2/$ feed—600 Nm^3/m^3 , WHSV—5 h^{-1} .

3. Experimental

3.1. Materials

Silicon carbide (SiC, Chelyabinsk Plant of Abrasive Materials, Chelyabinsk, Russia), silica (SiO₂, ChromAnalyt, Moscow, Russia), and alumina (γ-Al₂O₃, JSK Promkataliz, Ryazan, Russia) were obtained from commercial suppliers; the characteristics of these materials are presented in Table 3. Silica was crushed and sieved to 0.25–0.50 mm before the nickel phosphide supporting; silica and alumina grains with the size of 0.10–0.20 mm were used for catalyst dilution (without any special pretreatment). Ni(OAc)₂·4H₂O (Reakhim, Samara, Russia, ≥99%), (NH₄)₂HPO₄ (Alfa Aesar, Ward Hill, MA, USA, technical grade, P₂O₅ ≤ 53 wt %), HNO₃ (Reakhim, Samara, Russia, ≥70%) were used for the catalyst preparation. Methyl palmitate (C₁₅H₃₁COOCH₃, Sigma-Aldrich, St. Louis, MO, USA, ≥97%) was used as the reactant; *n*-dodecane (C₁₂H₂₆, Acros Organics, Morris Plains, NJ, USA, ≥99%) was used as the reaction medium. Methyl palmitate, palmitic acid (C₁₅H₃₁COOH, Across Organics, Morris Plains, NJ, USA, ≥98%), *n*-hexadecane (C₁₆H₃₄, Acros Organics, Morris Plains, NJ, USA, ≥99%), and *n*-pentadecane (C₁₅H₃₂, Acros Organics, Morris Plains, NJ, USA, ≥99%) were used as the standards to calibrate the flame ionization detector response for gas chromatography.

Table 3. Characteristics of silicon carbide, silica, and alumina.

Characteristics	SiC	SiO ₂	γ-Al ₂ O ₃
Shape	Grains	sphere	cylinder
Size of granules (mm)	0.1–0.2	4	4 × 1.5
S _{BET} (m ² /g)	1	300	235
D _{pore} (nm)	-	10.6	13.4
Pore volume (cm ³ /g)	-	0.80	0.79

3.2. Catalyst Synthesis

The silica-supported nickel phosphide catalyst was prepared by impregnation of silica with the solution of precursors followed by the drying, calcination, and temperature-programmed reduction (TPR). Silica grains (0.25–0.50 mm) were incipiently impregnated with an aqueous solution of Ni(CH₃COO)₂·4H₂O and (NH₄)₂HPO₄ that was stabilized by nitric acid, the concentrations of reagents were adjusted to obtain a catalyst containing about 2.5 wt % of Ni with the Ni/P ratio being equal to 0.5. The impregnated silica was dried at 110 °C for 4 h and then calcined at 500 °C for 4 h. The obtained precursor was reduced in the catalytic reactor in situ directly before the experiments. For the characterization of the catalyst by physicochemical methods, the precursor of the Ni₂P/SiO₂ catalyst was reduced ex situ in quartz tubular reactor in a stream of H₂ (150 mL/min per gram of precursor) at 600 °C (heating rate 3 °C/min up to 380 °C and then 1 °C/min until to 600 °C) for 3 h, and then cooled to the ambient temperature. Finally, the sample was passivated in a flow of 1% O₂/He (80 mL/min) for 1 h. The optimal conditions for the preparation of Ni₂P/SiO₂ samples from the phosphate precursor have been defined earlier [56,57].

3.3. Catalyst Characterization

The elemental analysis of the reduced catalysts and calcined precursors was performed using inductively coupled plasma atomic emission spectroscopy (ICP-AES) on Optima 4300 DV (Perkin Elmer, Villebon-sur-Yvette, France). The textural properties of the catalysts were determined using nitrogen physisorption at 77 K with an ASAP 2400 instrument (Micromeritics Instrument Corp., Norcross, GA, USA) within the partial pressure range 10⁻⁴–1.0. The catalysts were degassed at 250 °C for 12 h up to a residual pressure <10⁻¹ Pa before the measurements. Textural characteristics were calculated using a conventional method reported elsewhere [91].

XRD measurements were performed on an X-ray diffractometer Bruker D8 Advance (Bruker, Karlsruhe, Germany) using copper radiation ($\text{Cu K}\alpha$ —1.5418 Å) in the 2θ scanning range of 10–70°. The qualitative phase analysis was carried out using the JCPDS—International Centre for Diffraction Data database [92].

The samples were studied using transmission electron microscopy (TEM) with a JEM-2010 transmission electron microscope (JEOL, Tokyo, Japan) with an accelerating voltage of 200 kV and resolution of 0.14 nm. The local elemental composition was analyzed with an energy-dispersive EDX spectrometer, equipped with a Si (Li) detector (energy resolution—130 eV). To obtain statistical information, the structural parameters of ca. 300 particles were measured.

The acidic properties of the samples were analyzed by temperature-programmed desorption of ammonia (NH_3 -TPD), using an Autosorb-1 apparatus (Quantachrome Instruments, Boynton Beach, FL, USA) in the temperature range from 100 to 600 °C. Prior to adsorption of ammonia 0.25 g of each sample was reduced at 600 °C for 1 h in an H_2 flow (25 mL/min) and then cooled to 120 °C. Subsequently, the sample was saturated with NH_3 for 30 min. The physically adsorbed ammonia was desorbed from the sample with He flow (25 mL/min) at 120 °C for 30 min. Desorption of the chemically adsorbed part of ammonia was started by increasing the temperature from 120 °C up to 600 °C at a heating rate of 10 °C/min. The desorbed NH_3 was detected by a thermal conductivity detector.

3.4. Catalytic Experiments

The catalytic properties of $\text{Ni}_2\text{P}/\text{SiO}_2$ catalyst mixed with SiC, SiO_2 , or $\gamma\text{-Al}_2\text{O}_3$ in the HDO of the methyl palmitate (MP) were studied in the trickle-bed reactor (inner diameter—9 mm, length—265 mm). The catalytic properties of these systems were studied at hydrogen pressure 3.0 MPa, H_2 /feed volume ratio $600 \text{ Nm}^3/\text{m}^3$, and WHSV 5 h^{-1} (calculated as (mass of MP per h)/(mass of the catalyst)) in the temperature range of 250–330 °C. The dependence of product distribution on MP conversion was investigated at 270 °C varying WHSV in the range from 2 to 10 h^{-1} . The solution of methyl palmitate (10 wt % of MP corresponding to 1.183 wt % of oxygen) in *n*-dodecane was used in the experiments with *n*-octane as the internal standard.

The calcined precursor of $\text{Ni}_2\text{P}/\text{SiO}_2$ catalyst (0.5 mL, grain sizes—0.25–0.50 mm) was mixed with the SiC, SiO_2 , or $\gamma\text{-Al}_2\text{O}_3$ (4.1 mL, grain sizes—0.10–0.20 mm) and was loaded into the reactor. The catalyst precursor was reduced in situ in 60 mL/min H_2 flow and atmospheric pressure, the reactor was heated from room temperature to 380 °C (at 3 °C/min) and then to 600 °C (at 1 °C/min) and maintained at 600 °C for 3 h. After the reduction, the temperature was decreased to the reaction temperature and pressure was increased up to 3.0 MPa. Then the solvent was fed into the reactor that was replaced by the reaction mixture after the wetting of the catalyst during 1 h. The liquid products were collected every h until steady-state condition; the duration of each stage was not less than 6 h.

The reaction products were identified using a gas chromatography–mass spectrometry technique (GC-MS) produced by Agilent Technologies 7000 GC/MS Triple QQQ GC System 7890A (Santa Clara, CA, USA) with a VF-5MS quartz capillary column (30 m \times 0.25 mm \times 0.25 μm). Helium was used as the carrier gas with a constant flow of 1 mL/min. The sample (injection volume = 0.5 μL) was injected using the split mode (split ratio 1:50), with the injector temperature and GC-MS interface temperature, both at 300 °C. The column temperature was programmed: 50 °C for 10 min then from 50 to 300 °C at 10 °C/min. The MS scan interval was 0.2 s. The liquid samples were analyzed with a gas chromatography system (Agilent 6890N, Santa Clara, CA, USA) that was equipped with HP-1MS column (30 m \times 0.32 mm \times 1.0 μm) and flame ionization detector (FID). The contents of the components were calculated using absolute calibration factors for methyl palmitate, palmitic acid, *n*-pentadecane and *n*-hexadecane (Figures S2–S5 in Supplementary Materials). For hexadecanal, hexadecanol-1, hexadecanol-2 and palmityl palmitate we used efficient carbon number to calculate FID response factors. The carbon balance across the reactor for all experiments was >95%. The gas phase was analyzed using a Chromos GC-1000 chromatograph (Chromos, Dzerzhinsk, Russia), which was equipped with columns packed with 80/100 mesh HayeSep® (Sigma-Aldrich, St. Louis, MO, USA)

and FID. The concentrations of CO and CO₂ were determined with FID after the conversion of carbon oxides to methane in the methanator, containing a reduced Pd catalyst at 340 °C. The detection limit of the CO, CH₄, and CO₂ concentrations was 1 ppmv.

The total oxygen content in the reaction mixture was determined using CHNSO elemental analyzer Vario EL Cube (Elementar Analysensysteme GmbH, Hanau, Germany).

The conversion of methyl palmitate (X_{MP}), overall conversion of oxygen-containing compounds (X_{OCC}), and yield of *i*th compound ($Yield_i$) were calculated in accordance with the equations:

$$X_{MP} = \left(1 - \frac{n_{MP}}{n_{MP}^0}\right) \times 100\%, \quad (1)$$

$$X_{OCC} = \left(1 - \frac{n_O}{n_O^0}\right) \times 100\%, \quad (2)$$

$$Yield_i = \frac{n_i}{n_{MP}^0} \times 100\%, \quad (3)$$

where n_{MP}^0 and n_{MP} are the initial and current methyl palmitate content in the reaction mixture expressed in mol/L, n_O^0 and n_O are the initial and current oxygen content in the reaction mixture expressed in mol/L, n_i is the amount of *i*th compound in the product expressed in mol/L.

4. Conclusions

The behaviour of Ni₂P/SiO₂ catalyst taken in the mixture with the inert (SiC, SiO₂) or acidic (γ-Al₂O₃) material has been studied in methyl palmitate HDO. The catalytic activity of Ni₂P/SiO₂ catalyst increases significantly when γ-Al₂O₃ is used instead of SiC or SiO₂ for the catalyst dilution. Methyl palmitate conversion to the oxygenated intermediates is shown to be the rate-determining step over the Ni₂P/SiO₂-SiC and Ni₂P/SiO₂-SiO₂ systems, and can be increased due to the acceleration of ester hydrolysis over Lewis acid sites of alumina over Ni₂P/SiO₂-γ-Al₂O₃ system. Synergism of Ni₂P/SiO₂ and γ-Al₂O₃ physical mixture in methyl palmitate HDO has been explained by the cooperation of the metal sites of Ni₂P/SiO₂ and acid sites of γ-Al₂O₃ for metal- and acid-catalyzed reactions. The balancing of metal and acid sites via the change of Ni₂P/SiO₂ and γ-Al₂O₃ proportion in the reactor is shown to increase activity. The activity of the phosphide catalysts in the HDO of aliphatic ester can be improved by the employment of the support with the acidic properties, but the appropriate supporting procedure should be developed, which preserves the acidity of support during preparation. It is the upcoming challenge for the researchers because the precursors of phosphide catalysts have a tendency to interact with the non-inert support and deteriorate surface properties. The intentional use of observed synergism between metal sites of Ni₂P and acid sites of γ-Al₂O₃ in providing methyl palmitate HDO would play an important role in the development of the effective catalyst for the HDO of fatty acid esters over supported phosphide catalysts.

Supplementary Materials: The following are available online at www.mdpi.com/2073-4344/7/11/329/s1, Figure S1: TEM image of Ni₂P/SiO₂ catalyst reduced ex situ, Figure S2: GC FID calibration graph of methyl palmitate, Figure S3: GC FID calibration graph of palmitic acid, Figure S4: GC FID calibration graph of *n*-pentadecane, Figure S5: GC FID calibration graph of *n*-hexadecane.

Acknowledgments: This work was performed within the framework of budget project No. 0303-2016-0012 for Boreskov Institute of Catalysis. Ivan V. Shamanaev thanks the scientific council of Boreskov Institute of Catalysis for the scholarship support. The authors are grateful to Viktor A. Utkin and Mikhail V. Shashkov for reaction products identification using GC-MS technique.

Author Contributions: Galina A. Bukhtiyarova conceived and designed the experiments and supervised the work; Ivan V. Shamanaev performed the catalyst synthesis; Irina V. Deliy, Ivan V. Shamanaev and Pavel V. Aleksandrov performed the catalytic activity tests; Evgeny Yu. Gerasimov performed the catalyst characterization by TEM; Vera P. Pakharukova performed the catalyst characterization by XRD; Evgeny G. Kodenev performed the catalyst characterization by NH₃-TPD.

Conflicts of Interest: The authors declare no conflict of interest.

References

1. Kay Lup, A.N.; Abnisa, F.; Wan Daud, W.M.A.; Aroua, M.K. A review on reactivity and stability of heterogeneous metal catalysts for deoxygenation of bio-oil model compounds. *J. Ind. Eng. Chem.* **2017**. [[CrossRef](#)]
2. Si, Z.; Zhang, X.; Wang, C.; Ma, L.; Dong, R. An overview on catalytic hydrodeoxygenation of pyrolysis oil and its model compounds. *Catalysts* **2017**, *7*, 169. [[CrossRef](#)]
3. Choudhary, T.V.; Phillips, C.B. Renewable fuels via catalytic hydrodeoxygenation. *Appl. Catal. A* **2011**, *397*, 1–12. [[CrossRef](#)]
4. Serrano-Ruiz, J.C.; Ramos-Fernandez, E.V.; Sepulveda-Escribano, A. From biodiesel and bioethanol to liquid hydrocarbon fuels: New hydrotreating and advanced microbial technologies. *Energy Environ. Sci.* **2012**, *5*, 5638–5652. [[CrossRef](#)]
5. Hachemi, I.; Jenistova, K.; Maki-Arvela, P.; Kumar, N.; Eranen, K.; Hemming, J.; Murzin, D.Y. Comparative study of sulfur-free nickel and palladium catalysts in hydrodeoxygenation of different fatty acid feedstocks for production of biofuels. *Catal. Sci. Technol.* **2016**, *6*, 1476–1487. [[CrossRef](#)]
6. Serrano-Ruiz, J.C. Biomass conversion technologies: Catalytic conversion technologies. In *Biorefineries: Targeting Energy, High Value Products and Waste Valorisation*; Rabaçal, M., Ferreira, A.F., Silva, C.A.M., Costa, M., Eds.; Springer International Publishing: Cham, Switzerland, 2017; pp. 113–121.
7. Kay Lup, A.N.; Abnisa, F.; Daud, W.M.A.W.; Aroua, M.K. A review on reaction mechanisms of metal-catalyzed deoxygenation process in bio-oil model compounds. *Appl. Catal. A* **2017**, *541*, 87–106. [[CrossRef](#)]
8. Li, D.; Xin, H.; Du, X.; Hao, X.; Liu, Q.; Hu, C. Recent advances for the production of hydrocarbon biofuel via deoxygenation progress. *Sci. Bull.* **2015**, *60*, 2096–2106. [[CrossRef](#)]
9. Mikulec, J.; Cvengros, J.; Jorikova, L.; Banic, M.; Kleinova, A. Second generation diesel fuel from renewable sources. *J. Clean. Prod.* **2010**, *18*, 917–926. [[CrossRef](#)]
10. Hari, T.K.; Yaakob, Z. Production of diesel fuel by the hydrotreatment of jatropha oil derived fatty acid methyl esters over gamma-Al₂O₃ and SiO₂ supported NiCo bimetallic catalysts. *React. Kinet. Mech. Catal.* **2015**, *116*, 131–145. [[CrossRef](#)]
11. Hari, T.K.; Yaakob, Z. CoFe/gamma-Al₂O₃ Catalyst for the hydrotreatment of fatty acid methyl esters (FAME). *Chem. Lett.* **2015**, *44*, 1237–1239. [[CrossRef](#)]
12. Al-Sabawi, M.; Chen, J.W. Hydroprocessing of biomass-derived oils and their blends with petroleum feedstocks: A review. *Energy Fuels* **2012**, *26*, 5373–5399. [[CrossRef](#)]
13. Kanda, Y.; Matsukura, Y.; Sawada, A.; Sugioka, M.; Uemichi, Y. Low-temperature synthesis of rhodium phosphide on alumina and investigation of its catalytic activity toward the hydrodesulfurization of thiophene. *Appl. Catal. A* **2016**, *515*, 25–31. [[CrossRef](#)]
14. Guan, Q.X.; Wan, F.F.; Han, F.; Liu, Z.H.; Li, W. Hydrodeoxygenation of methyl palmitate over MCM-41 supported nickel phosphide catalysts. *Catal. Today* **2016**, *259*, 467–473. [[CrossRef](#)]
15. Kubicka, D.; Kaluza, L. Deoxygenation of vegetable oils over sulfided Ni, Mo and NiMo catalysts. *Appl. Catal. A* **2010**, *372*, 199–208. [[CrossRef](#)]
16. Donnis, B.; Egeberg, R.G.; Blom, P.; Knudsen, K.G. Hydroprocessing of bio-oils and oxygenates to hydrocarbons. Understanding the reaction routes. *Top. Catal.* **2009**, *52*, 229–240. [[CrossRef](#)]
17. Simacek, P.; Kubicka, D.; Kubickova, I.; Homola, F.; Pospisil, M.; Chudoba, J. Premium quality renewable diesel fuel by hydroprocessing of sunflower oil. *Fuel* **2011**, *90*, 2473–2479. [[CrossRef](#)]
18. Lapuerta, M.; Villajos, M.; Agudelo, J.R.; Boehman, A.L. Key properties and blending strategies of hydrotreated vegetable oil as biofuel for diesel engines. *Fuel Process. Technol.* **2011**, *92*, 2406–2411. [[CrossRef](#)]
19. Furimsky, E. Hydroprocessing challenges in biofuels production. *Catal. Today* **2013**, *217*, 13–56. [[CrossRef](#)]
20. Laurent, E.; Delmon, B. Study of the hydrodeoxygenation of carbonyl, carboxylic and guaiacyl groups over sulfided como/gamma-Al₂O₃ and nimo/gamma-Al₂O₃ catalyst. 2. Influence of water, ammonia and hydrogen-sulfide. *Appl. Catal. A* **1994**, *109*, 97–115. [[CrossRef](#)]
21. Senol, O.I.; Viljava, T.R.; Krause, A.O.I. Hydrodeoxygenation of methyl esters on sulphided NiMo/gamma-Al₂O₃ and CoMo/gamma-Al₂O₃ catalysts. *Catal. Today* **2005**, *100*, 331–335. [[CrossRef](#)]

22. Senol, O.I.; Ryymin, E.-M.; Viljava, T.-R.; Krause, A.O.I. Reactions of methyl heptanoate hydrodeoxygenation on sulphided catalysts. *J. Mol. Catal. Chem.* **2007**, *268*, 1–8. [[CrossRef](#)]
23. Coumans, A.E.; Hensen, E.J.M. A real support effect on the hydrodeoxygenation of methyl oleate by sulfided NiMo catalysts. *Catal. Today* **2017**. [[CrossRef](#)]
24. Itthibenchapong, V.; Srifa, A.; Kaewmeesri, R.; Kidkhunthod, P.; Faungnawakij, K. Deoxygenation of palm kernel oil to jet fuel-like hydrocarbons using Ni-MoS₂/γ-Al₂O₃ catalysts. *Energy Convers. Manag.* **2017**, *134*, 188–196. [[CrossRef](#)]
25. Bie, Y.W.; Gutierrez, A.; Viljava, T.R.; Kanervo, J.M.; Lehtonen, J. Hydrodeoxygenation of methyl heptanoate over noble metal catalysts: Catalyst screening and reaction network. *Ind. Eng. Chem. Res.* **2013**, *52*, 11544–11551. [[CrossRef](#)]
26. Ma, B.; Zhao, C. High-grade diesel production by hydrodeoxygenation of palm oil over a hierarchically structured Ni/HBEA catalyst. *Green Chem.* **2015**, *17*, 1692–1701. [[CrossRef](#)]
27. Kon, K.; Onodera, W.; Takakusagi, S.; Shimizu, K. Hydrodeoxygenation of fatty acids and triglycerides by Pt-loaded Nb₂O₅ catalysts. *Catal. Sci. Technol.* **2014**, *4*, 3705–3712. [[CrossRef](#)]
28. Madsen, A.T.; Ahmed, E.; Christensen, C.H.; Fehrmann, R.; Riisager, A. Hydrodeoxygenation of waste fat for diesel production: Study on model feed with Pt/alumina catalyst. *Fuel* **2011**, *90*, 3433–3438. [[CrossRef](#)]
29. Goto, H.; Takagaki, A.; Kikuchi, R.; Oyama, S.T. Hydrogenation of 2,5-dimethylfuran on hexagonal-boron nitride- and silica-supported platinum catalysts. *Appl. Catal. A* **2017**. [[CrossRef](#)]
30. Senol, O.I.; Ryymin, E.M.; Viljava, T.R.; Krause, A.O.I. Effect of hydrogen sulphide on the hydrodeoxygenation of aromatic and aliphatic oxygenates on sulphided catalysts. *J. Mol. Catal. Chem.* **2007**, *277*, 107–112. [[CrossRef](#)]
31. Pinheiro, A.; Dupassieux, N.; Hudebine, D.; Geantet, C. Impact of the presence of carbon monoxide and carbon dioxide on gas oil hydrotreatment: Investigation on liquids from biomass cotreatment with petroleum cuts. *Energy Fuels* **2011**, *25*, 804–812. [[CrossRef](#)]
32. Philippe, M.; Richard, F.; Hudebine, D.; Brunet, S. Transformation of dibenzothiophenes model molecules over CoMoP/Al₂O₃ catalyst in the presence of oxygenated compounds. *Appl. Catal. B* **2013**, *132*, 493–498. [[CrossRef](#)]
33. Vlasova, E.N.; Deliy, I.V.; Nuzhdin, A.L.; Aleksandrov, P.V.; Gerasimov, E.Y.; Aleshina, G.I.; Bukhtiyarova, G.A. Catalytic properties of CoMo/Al₂O₃ sulfide catalysts in the hydrorefining of straight-run diesel fraction mixed with rapeseed oil. *Kinet. Catal.* **2014**, *55*, 481–491. [[CrossRef](#)]
34. Ochoa-Hernandez, C.; Yang, Y.X.; Pizarro, P.; O'Shea, V.A.D.; Coronado, J.M.; Serrano, D.P. Hydrocarbons production through hydrotreating of methyl esters over Ni and Co supported on SBA-15 and Al-SBA-15. *Catal. Today* **2013**, *210*, 81–88. [[CrossRef](#)]
35. Loe, R.; Santillan-Jimenez, E.; Morgan, T.; Sewell, L.; Ji, Y.Y.; Jones, S.; Isaacs, M.A.; Lee, A.F.; Crocker, M. Effect of Cu and Sn promotion on the catalytic deoxygenation of model and algal lipids to fuel-like hydrocarbons over supported Ni catalysts. *Appl. Catal. B* **2016**, *191*, 147–156. [[CrossRef](#)]
36. Kukushkin, R.G.; Bulavchenko, O.A.; Kaichev, V.V.; Yakovlev, V.A. Influence of Mo on catalytic activity of Ni-based catalysts in hydrodeoxygenation of esters. *Appl. Catal. B* **2015**, *163*, 531–538. [[CrossRef](#)]
37. Yakovlev, V.A.; Khromova, S.A.; Sherstyuk, O.V.; Dundich, V.O.; Ermakov, D.Y.; Novopashina, V.M.; Lebedev, M.Y.; Bulavchenko, O.; Parmon, V.N. Development of new catalytic systems for upgraded bio-fuels production from bio-crude-oil and biodiesel. *Catal. Today* **2009**, *144*, 362–366. [[CrossRef](#)]
38. Zuo, H.L.; Liu, Q.Y.; Wang, T.J.; Ma, L.L.; Zhang, O.; Zhang, Q. Hydrodeoxygenation of methyl palmitate over supported Ni catalysts for diesel-like fuel production. *Energy Fuels* **2012**, *26*, 3747–3755. [[CrossRef](#)]
39. Pan, Z.; Wang, R.; Chen, J. Deoxygenation of methyl laurate as a model compound on Ni-Zn alloy and intermetallic compound catalysts: Geometric and electronic effects of oxophilic Zn. *Appl. Catal. B* **2017**. [[CrossRef](#)]
40. Wang, H.Y.; Jiao, T.T.; Li, Z.X.; Li, C.S.; Zhang, S.J.; Zhang, J.L. Study on palm oil hydrogenation for clean fuel over Ni-Mo-W/γ-Al₂O₃-ZSM-5 catalyst. *Fuel Process. Technol.* **2015**, *139*, 91–99. [[CrossRef](#)]
41. Hollak, S.A.W.; Gosselink, R.W.; van Es, D.S.; Bitter, J.H. Comparison of tungsten and molybdenum carbide catalysts for the hydrodeoxygenation of oleic acid. *ACS Catal.* **2013**, *3*, 2837–2844. [[CrossRef](#)]
42. Wang, H.L.; Yan, S.L.; Salley, S.O.; Ng, K.Y.S. Support effects on hydrotreating of soybean oil over NiMo carbide catalyst. *Fuel* **2013**, *111*, 81–87. [[CrossRef](#)]

43. Monnier, J.; Sulimma, H.; Dalai, A.; Caravaggio, G. Hydrodeoxygenation of oleic acid and canola oil over alumina-supported metal nitrides. *Appl. Catal. A* **2010**, *382*, 176–180. [[CrossRef](#)]
44. Chen, J.X.; Shi, H.; Li, L.; Li, K.L. Deoxygenation of methyl laurate as a model compound to hydrocarbons on transition metal phosphide catalysts. *Appl. Catal. B* **2014**, *144*, 870–884. [[CrossRef](#)]
45. Chen, J.X.; Yang, Y.; Shi, H.; Li, M.F.; Chu, Y.; Pan, Z.Y.; Yu, X.B. Regulating product distribution in deoxygenation of methyl laurate on silica-supported Ni-Mo phosphides: Effect of Ni/Mo ratio. *Fuel* **2014**, *129*, 1–10. [[CrossRef](#)]
46. Shi, H.; Chen, J.X.; Yang, Y.; Tian, S.S. Catalytic deoxygenation of methyl laurate as a model compound to hydrocarbons on nickel phosphide catalysts: Remarkable support effect. *Fuel Process. Technol.* **2014**, *118*, 161–170. [[CrossRef](#)]
47. Yang, Y.; Chen, J.X.; Shi, H. Deoxygenation of methyl laurate as a model compound to hydrocarbons on Ni₂P/SiO₂, Ni₂P/MCM-41, and Ni₂P/SBA-15 catalysts with different dispersions. *Energy Fuels* **2013**, *27*, 3400–3409. [[CrossRef](#)]
48. Yang, Y.X.; Ochoa-Hernandez, C.; O’Shea, V.A.D.; Coronado, J.M.; Serrano, D.P. Ni₂P/SBA-15 As a hydrodeoxygenation catalyst with enhanced selectivity for the conversion of methyl oleate into *n*-octadecane. *ACS Catal.* **2012**, *2*, 592–598. [[CrossRef](#)]
49. Yang, Y.X.; Ochoa-Hernandez, C.; Pizarro, P.; O’Shea, V.A.D.; Coronado, J.M.; Serrano, D.P. Synthesis of nickel phosphide nanorods as catalyst for the hydrotreating of methyl oleate. *Top. Catal.* **2012**, *55*, 991–998. [[CrossRef](#)]
50. Yang, Y.X.; Ochoa-Hernandez, C.; Pizarro, P.; O’Shea, V.A.D.; Coronado, J.M.; Serrano, D.P. Influence of the Ni/P ratio and metal loading on the performance of Ni_xP_y/SBA-15 catalysts for the hydrodeoxygenation of methyl oleate. *Fuel* **2015**, *144*, 60–70. [[CrossRef](#)]
51. Zarchin, R.; Rabaev, M.; Vidruk-Nehemya, R.; Landau, M.V.; Herskowitz, M. Hydroprocessing of soybean oil on nickel-phosphide supported catalysts. *Fuel* **2015**, *139*, 684–691. [[CrossRef](#)]
52. Pan, Z.Y.; Wang, R.J.; Li, M.F.; Chu, Y.; Chen, J.X. Deoxygenation of methyl laurate to hydrocarbons on silica-supported Ni-Mo phosphides: Effect of calcination temperatures of precursor. *J. Energy Chem.* **2015**, *24*, 77–86. [[CrossRef](#)]
53. Xue, Y.A.; Guan, Q.X.; Li, W. Synthesis of bulk and supported nickel phosphide using microwave radiation for hydrodeoxygenation of methyl palmitate. *RSC Adv.* **2015**, *5*, 53623–53628. [[CrossRef](#)]
54. Peroni, M.; Lee, I.; Huang, X.; Barath, E.; Gutiérrez, O.Y.; Lercher, J.A. Deoxygenation of palmitic acid on unsupported transition metal phosphides. *ACS Catal.* **2017**. [[CrossRef](#)]
55. Zheng, Z.; Li, M.F.; Chu, Y.; Chen, J.X. Influence of CS₂ on performance of Ni₂P/SiO₂ for deoxygenation of methyl laurate as a model compound to hydrocarbons: Simultaneous investigation on catalyst deactivation. *Fuel Process. Technol.* **2015**, *134*, 259–269. [[CrossRef](#)]
56. Shamanaev, I.V.; Deliy, I.V.; Pakharukova, V.P.; Gerasimov, E.Y.; Rogov, V.A.; Bukhtiyarova, G.A. Effect of the preparation conditions on the physicochemical and catalytic properties of Ni₂P/SiO₂ catalysts. *Russ. Chem. Bull.* **2015**, *64*, 2361–2370. [[CrossRef](#)]
57. Shamanaev, I.V.; Deliy, I.V.; Aleksandrov, P.V.; Gerasimov, E.Y.; Pakharukova, V.P.; Kodenev, E.G.; Ayupov, A.B.; Andreev, A.S.; Lapina, O.B.; Bukhtiyarova, G.A. Effect of precursor on the catalytic properties of Ni₂P/SiO₂ in methyl palmitate hydrodeoxygenation. *RSC Adv.* **2016**, *6*, 30372–30383. [[CrossRef](#)]
58. Alvarez-Galvan, M.C.; Blanco-Brieva, G.; Capel-Sanchez, M.; Morales-delaRosa, S.; Campos-Martin, J.M.; Fierro, J.L.G. Metal phosphide catalysts for the hydrotreatment of non-edible vegetable oils. *Catal. Today* **2017**. [[CrossRef](#)]
59. Liu, X.; Li, Z.; Zhang, B.; Hu, M. Improvement of hydrodeoxygenation stability of nickel phosphide based catalysts by silica modification as structural promoter. *Fuel* **2017**, *204*, 144–151. [[CrossRef](#)]
60. Zhao, S.; Zhang, Z.; Zhu, K.; Chen, J. Hydroconversion of methyl laurate on bifunctional Ni₂P/AlMCM-41 catalyst prepared via in situ phosphorization using triphenylphosphine. *Appl. Surf. Sci.* **2017**, *404*, 388–397. [[CrossRef](#)]
61. Xin, H.; Guo, K.; Li, D.; Yang, H.; Hu, C. Production of high-grade diesel from palmitic acid over activated carbon-supported nickel phosphide catalysts. *Appl. Catal. B* **2016**, *187*, 375–385. [[CrossRef](#)]
62. Pan, Z.; Wang, R.; Nie, Z.; Chen, J. Effect of a second metal (Co, Fe, Mo and W) on performance of Ni₂P/SiO₂ for hydrodeoxygenation of methyl laurate. *J. Energy Chem.* **2016**, *25*, 418–426. [[CrossRef](#)]

63. Guan, Q.X.; Han, F.; Li, W. Catalytic performance and deoxygenation path of methyl palmitate on Ni₂P/SiO₂ synthesized using the thermal decomposition of nickel hypophosphite. *RSC Adv.* **2016**, *6*, 31308–31315. [[CrossRef](#)]
64. Chen, J.; Han, M.; Zhao, S.; Pan, Z.; Zhang, Z. An in situ approach to preparing Ni₂P/SiO₂ catalyst under mild conditions and its performance for the deoxygenation of methyl laurate to hydrocarbons. *Catal. Sci. Technol.* **2016**, *6*, 3938–3949. [[CrossRef](#)]
65. Zhang, Z.; Tang, M.; Chen, J. Effects of P/Ni ratio and Ni content on performance of γ -Al₂O₃-supported nickel phosphides for deoxygenation of methyl laurate to hydrocarbons. *Appl. Surf. Sci.* **2016**, *360 Pt A*, 353–364. [[CrossRef](#)]
66. Liu, C.-Y.; Yang, H.; Jing, Z.-Y.; Xi, K.-Z.; Qiao, C.-Z. Hydrodeoxygenation of fatty acid methyl esters and isomerization of products over NiP/SAPO-11 catalysts. *J. Fuel Chem. Technol.* **2016**, *44*, 1211–1216. [[CrossRef](#)]
67. Luo, N.; Cao, Y.; Li, J.; Guo, W.; Zhao, Z.-W. Preparation of Ni₂P/Zr-MCM-41 catalyst and its performance in the hydrodeoxygenation of Jatropha curcas oil. *J. Fuel Chem. Technol.* **2016**, *44*, 76–83. [[CrossRef](#)]
68. Lee, S.I.; Kim, D.W.; Jeon, H.J.; Ju, S.J.; Ryu, J.W.; Oh, S.H.; Koh, J.H. Metal Phosphorus Compound for Preparing Biodiesel and Method Preparing Biodiesel Using the Same. Patent No. US2014/0150332A1, 5 June 2014.
69. Gosselink, R.W.; Hollak, S.A.W.; Chang, S.W.; van Haveren, J.; de Jong, K.P.; Bitter, J.H.; van Es, D.S. Reaction pathways for the deoxygenation of vegetable oils and related model compounds. *ChemSusChem* **2013**, *6*, 1576–1594. [[CrossRef](#)] [[PubMed](#)]
70. Huber, G.W.; O'Connor, P.; Corma, A. Processing biomass in conventional oil refineries: Production of high quality diesel by hydrotreating vegetable oils in heavy vacuum oil mixtures. *Appl. Catal. A* **2007**, *329*, 120–129. [[CrossRef](#)]
71. Deliy, I.V.; Vlasova, E.N.; Nuzhdin, A.L.; Gerasimov, E.Y.; Bukhtiyarova, G.A. Hydrodeoxygenation of methyl palmitate over sulfided Mo/Al₂O₃, CoMo/Al₂O₃ and NiMo/Al₂O₃ catalysts. *RSC Adv.* **2014**, *4*, 2242–2250. [[CrossRef](#)]
72. Prins, R.; Bussell, M.E. Metal phosphides: preparation, characterization and catalytic reactivity. *Catal. Lett.* **2012**, *142*, 1413–1436. [[CrossRef](#)]
73. Liu, X.G.; Xu, L.; Zhang, B.Q. Essential elucidation for preparation of supported nickel phosphide upon nickel phosphate precursor. *J. Solid State Chem.* **2014**, *212*, 13–22. [[CrossRef](#)]
74. Peroni, M.; Mancino, G.; Baráth, E.; Gutiérrez, O.Y.; Lercher, J.A. Bulk and γ -Al₂O₃-supported Ni₂P and MoP for hydrodeoxygenation of palmitic acid. *Appl. Catal. B* **2016**, *180*, 301–311. [[CrossRef](#)]
75. Oyama, S.; Wang, X.; Lee, Y.; Bando, K.; Requejo, F. Effect of phosphorus content in nickel phosphide catalysts studied by XAFS and other techniques. *J. Catal.* **2002**, *210*, 207–217. [[CrossRef](#)]
76. Cecilia, J.; Infantes-Molina, A.; Rodriguez-Castellon, E.; Jimenez-Lopez, A. A novel method for preparing an active nickel phosphide catalyst for HDS of dibenzothiophene. *J. Catal.* **2009**, *263*, 4–15. [[CrossRef](#)]
77. Stinner, C.; Prins, R.; Weber, T. Binary and ternary transition-metal phosphides as HDN catalysts. *J. Catal.* **2001**, *202*, 187–194. [[CrossRef](#)]
78. Berhault, G.; Afanasiev, P.; Loboue, H.; Geantet, C.; Cseri, T.; Pichon, C.; Guillot-Deudon, C.; Lafond, A. In Situ XRD, XAS, and magnetic susceptibility study of the reduction of ammonium nickel phosphate NiNH₄PO₄ center dot H₂O into nickel phosphide. *Inorg. Chem.* **2009**, *48*, 2985–2992. [[CrossRef](#)] [[PubMed](#)]
79. Stinner, C.; Tang, Z.; Haouas, M.; Weber, T.; Prins, R. Preparation and P-31 NMR characterization of nickel phosphides on silica. *J. Catal.* **2002**, *208*, 456–466. [[CrossRef](#)]
80. Liu, D.P.; Wang, A.J.; Liu, C.G.; Prins, R. Bulk and Al₂O₃-supported Ni₂P HDS catalysts prepared by separating the nickel and hypophosphite sources. *Catal. Commun.* **2016**, *77*, 13–17. [[CrossRef](#)]
81. Li, D.P.; Wang, A.J.; Liu, C.G.; Prins, R. Ni₂P/Al₂O₃ hydrodesulfurization catalysts prepared by separating the nickel compound and hypophosphite. *Catal. Today* **2017**, *292*, 133–142. [[CrossRef](#)]
82. Wu, S.K.; Lai, P.C.; Lin, Y.C. Atmospheric Hydrodeoxygenation of guaiacol over nickel phosphide catalysts: Effect of phosphorus composition. *Catal. Lett.* **2014**, *144*, 878–889. [[CrossRef](#)]
83. Lee, Y.K.; Oyama, S.T. Bifunctional nature of a SiO₂-supported Ni₂P catalyst for hydrotreating: EXAFS and FTIR studies. *J. Catal.* **2006**, *239*, 376–389. [[CrossRef](#)]
84. Cecilia, J.A.; Infantes-Molina, A.; Rodriguez-Castellon, E.; Jimenez-Lopez, A.; Oyama, S.T. Oxygen-removal of dibenzofuran as a model compound in biomass derived bio-oil on nickel phosphide catalysts: Role of phosphorus. *Appl. Catal. B* **2013**, *136*, 140–149. [[CrossRef](#)]

85. Berteau, P.; Delmon, B. Modified aluminas—Relationship between activity in 1-butanol dehydration and acidity measured by NH₃ TPD. *Catal. Today* **1989**, *5*, 121–137. [[CrossRef](#)]
86. Kijeński, J.; Baiker, A. Acidic sites on catalyst surfaces and their determination. *Catal. Today* **1989**, *5*, 1–120. [[CrossRef](#)]
87. Turek, W.; Haber, J.; Krowiak, A. Dehydration of isopropyl alcohol used as an indicator of the type and strength of catalyst acid centres. *Appl. Surf. Sci.* **2005**, *252*, 823–827. [[CrossRef](#)]
88. Han, F.; Guan, Q.; Li, W. Deoxygenation of methyl palmitate over SiO₂-supported nickel phosphide catalysts: Effects of pressure and kinetic investigation. *RSC Adv.* **2015**, *5*, 107533–107539. [[CrossRef](#)]
89. Liu, Y.H.; Yao, L.; Xin, H.; Wang, G.S.; Li, D.; Hu, C.W. The production of diesel-like hydrocarbons from palmitic acid over HZSM-22 supported nickel phosphide catalysts. *Appl. Catal. B* **2015**, *174*, 504–514. [[CrossRef](#)]
90. Prins, R. Hydrogen spillover. facts and fiction. *Chem. Rev.* **2012**, *112*, 2714–2738. [[CrossRef](#)] [[PubMed](#)]
91. Fenelonov, V.B.; Romannikov, V.N.; Derevyankin, A.Y. Mesopore size and surface area calculations for hexagonal mesophases (types MCM-41, FSM-16, etc.) using low-angle XRD and adsorption data. *Microporous Mesoporous Mater.* **1999**, *28*, 57–72. [[CrossRef](#)]
92. *International Centre for Diffraction Data (ICDD)*; Fachinformationszentrum (FIZ): Karlsruhe, Germany, 2011.



© 2017 by the authors. Licensee MDPI, Basel, Switzerland. This article is an open access article distributed under the terms and conditions of the Creative Commons Attribution (CC BY) license (<http://creativecommons.org/licenses/by/4.0/>).